A&A 611, A61 (2018)
https://doi.org/10.1051/0004-6361/201731796

Astronomy & Astrophysics

Challenges in the determination of the interstellar flow longitude from the pickup ion cutoff

A. Taut[1], L. Berger[1], E. Möbius[2], C. Drews[1], V. Heidrich-Meisner[1], D. Keilbach[1], M. A. Lee[2], and R. F. Wimmer-Schweingruber[1]

[1] Institut für Experimentelle und Angewandte Physik, Christian-Albrechts-Universität zu Kiel, Kiel, Germany
e-mail: taut@physik.uni-kiel.de
[2] Space Science Center & Department of Physics, University of New Hampshire, Durham, NH, USA

Received 18 August 2017 / Accepted 20 November 2017

ABSTRACT

Context. The interstellar flow longitude corresponds to the Sun's direction of movement relative to the local interstellar medium. Thus, it constitutes a fundamental parameter for our understanding of the heliosphere and, in particular, its interaction with its surroundings, which is currently investigated by the Interstellar Boundary EXplorer (IBEX). One possibility to derive this parameter is based on pickup ions (PUIs) that are former neutral ions that have been ionized in the inner heliosphere. The neutrals enter the heliosphere as an interstellar wind from the direction of the Sun's movement against the partially ionized interstellar medium. PUIs carry information about the spatial variation of their neutral parent population (density and flow vector field) in their velocity distribution function. From the symmetry of the longitudinal flow velocity distribution, the interstellar flow longitude can be derived.
Aims. The aim of this paper is to identify and eliminate systematic errors that are connected to this approach of measuring the interstellar flow longitude; we want to minimize any systematic influences on the result of this analysis and give a reasonable estimate for the uncertainty.
Methods. We use He^+ data measured by the PLAsma and SupraThermal Ion Composition (PLASTIC) sensor on the Solar TErrestrial RElations Observatory Ahead (STEREO A) spacecraft. We analyze a recent approach, identify sources of systematic errors, and propose solutions to eliminate them. Furthermore, a method is introduced to estimate the error associated with this approach. Additionally, we investigate how the selection of interplanetary magnetic field angles, which is closely connected to the pickup ion velocity distribution function, affects the result for the interstellar flow longitude.
Results. We find that the revised analysis used to address part of the expected systematic effects obtains significantly different results than presented in the previous study. In particular, the derived uncertainties are considerably larger. Furthermore, an unexpected systematic trend of the resulting interstellar flow longitude with the selection of interplanetary magnetic field orientation is uncovered.

Key words. Sun: heliosphere – Sun: fundamental parameters – ISM: general – solar wind

1. Context

The heliosphere is a plasma bubble that is carved out of the partially ionized local interstellar medium (LISM) by the solar wind. Recently, our understanding of the boundaries of the heliosphere and its interaction with the LISM has been expanded by the unexpected results of the Interstellar Boundary EXplorer (IBEX) and the in situ observations by the Voyager spacecraft (Stone et al. 2005). Among the findings is the IBEX ribbon (McComas et al. 2009), which provides insight into the interstellar magnetic field. Another key component of the interaction is the interstellar flow vector, $\boldsymbol{v}_{\rm LISM}$, which denotes the relative motion between the Sun and the LISM. Therefore, the interstellar flow vector has been the objective of investigations for years (Axford 1972). First, remote measurements of neutral hydrogen (Bertaux & Blamont 1971) and helium (Weller & Meier 1974) were performed using backscattered solar UV observations. Later on, in situ measurements using pickup ions (PUIs) (Möbius et al. 1995) and direct neutral particle observations (Witte 2004) complemented the previous studies. A more extensive summary of the history of the investigation of the interstellar flow can be found in Möbius et al. (2004).

Due to the relative motion between the Sun and the LISM of ~26 km s^{-1} (Wood et al. 2015), neutral particles enter the heliosphere as an interstellar wind from a defined direction. Since 2008, these neutrals are measured by IBEX amongst others, from which one can derive $\boldsymbol{v}_{\rm LISM}$ and the temperature of the interstellar neutral flow, $T_{\rm ISN}$, through the hyperbolic trajectory equation (see Bzowski et al. 2012; Möbius et al. 2012). The inflow vector can also be expressed by the inflow longitude, $\lambda_{\rm flow}$; latitude, $\beta_{\rm flow}$; and speed, $V_{\rm ISN}$. However, these parameters are coupled. They can be expressed as a function of the interstellar neutral flow longitude and the range of allowable parameters along the 4D parameter tube is relatively large (see Schwadron et al. 2015). Therefore, an independent measurement of the interstellar flow longitude would help to constrain this parameter tube.

The interstellar neutral flow forms a characteristic structure close to the Sun that is symmetric about the flow direction. Not only its density profile, but also its velocity pattern follows this symmetry, which is obvious along a circular orbit around the Sun. From these features the longitudinal direction of the flow vector can be derived using interstellar PUI measurements. Interstellar PUIs are created from interstellar wind neutrals by

ionization processes, such as photoionization by EUV radiation, charge-exchange with solar wind protons, and electron impact. PUI were already predicted in the 1970s by Fahr (1971) and subsequently confirmed by observations of the AMPTE spacecraft (Möbius et al. 1985). One can easily identify PUIs by their almost exclusive single-charge state and their highly suprathermal velocity distribution function (VDF), which is a consequence of the pickup process. Once ionized, PUIs are exposed to the electromagnetic forces exerted by the solar wind and the frozen-in magnetic field, and transported outward.

As the interstellar wind is gravitationally focused downwind of the Sun, a region of enhanced neutral density evolves, called the focusing cone. Of course, the condition for this structure to form is that enough neutrals reach the downwind side without being ionized. Hence, the focusing cone is only observed for elements with a high first ionization potential, such as helium or neon (Drews et al. 2010). On the upwind side of the Sun, called the crescent, forms for elements with a low first ionization potential like oxygen (Drews et al. 2012). At ecliptic longitudes, λ, which corresponds to the interstellar upwind direction, the neutrals have a smaller pathlength to reach a distance of 1 AU from the Sun. Thus, these neutrals are less affected by ionization processes, which increases the number of particles that reach this distance.

These two regions are aligned with the interstellar flow longitude, $\lambda_{\rm flow}$. The PUI production rate is directly coupled to the neutral particle density and thus largely reproduces the focusing cone and the crescent. Furthermore, the crescent signature is more pronounced in the observed PUI flux due to the radial velocity variation that follows the density profile (Sokół et al. 2016). In this way, the crescent also becomes visible for species with low ionization rates, such as helium. Hence, PUI measurements can also be utilized to determine $\lambda_{\rm flow}$, as was performed in Drews et al. (2012). Although a careful error estimation was performed, it is likely that these results are affected by systematic errors. In contrast to neutrals, PUIs are affected by transport effects that act preferably along the mean interplanetary magnetic field (IMF), which follows the Parker spiral (Chalov 2014; Quinn et al. 2016).

Another method for using PUIs as a diagnostic tool to derive the interstellar flow longitude, $\lambda_{\rm flow}$, was recently proposed by Möbius et al. (2015). As shown in Möbius et al. (1999) the injection speed of PUIs into the solar wind depends on ecliptic longitude because of the longitude-dependant relative motion of the neutral interstellar wind particles and the radially outward streaming solar wind. This injection speed can be determined from the PUI VDF by utilizing what is known as the cutoff feature. As this method is based on the evaluation of freshly injected ions, it is expected to be less sensitive to transport effects and therefore substantially less affected by the possibility of a strong systematic error.

2. Motivation and goals

In this paper we revisit the method presented as a proof-of-concept study by Möbius et al. (2015) using He^+ PUI data from the PLAsma and SupraThermal Ion Composition instrument (PLASTIC; Galvin et al. (2008)) on board the Solar TErrestrial RElations Observatory Ahead spacecraft (STEREO A). We extend this method by analyzing its weaknesses and proposing ways to circumvent these disadvantages. Furthermore, a new method to obtain a reasonable error estimation is applied. Using the improved method to derive the interstellar flow longitude, we investigate further systematic effects that may influence the interstellar flow longitude results from the He^+ PUI cutoff.

First, we give a short introduction into the STEREO A/PLASTIC He^+ data. Second, we provide an overview of the PUI physics that enables the determination of the interstellar flow longitude from PUI VDFs, which was performed in Möbius et al. (2015). We summarize the individual steps of the revisited analysis and describe the improvements implemented in each step.

As in Möbius et al. (2015) we perform the PUI analysis in the solar wind frame. This has the advantage that the injection speed of PUIs is solely a function of the solar wind speed, $|\boldsymbol{v}_{\rm sw}| = v_{\rm sw}$, and the local interstellar neutral flow velocity, $\boldsymbol{V}_n$. In Fig. 1 this is illustrated for the simplified case of PUIs that are created from neutrals that are at rest. Due to their gyration about the IMF, the PUI velocities lie on a shell that has the radius of the solar wind speed and is centered around the solar wind velocity. Accordingly, all PUIs of the torus VDF move at solar wind speed in the solar wind frame in this case.

Möbius et al. (2015) perform their analysis of the PUI distribution in terms of the normalized PUI speed $w'_{\rm He^+} = \frac{v'_{\rm He^+}}{v_{\rm sw}}$, where $v'_{\rm He^+} = |\boldsymbol{v}_{\rm He^+} - \boldsymbol{v}_{\rm sw}|$ is the PUI speed in the solar wind frame. In contrast, we transform the measured PUI speeds into another data product, V_r, which eliminates the influence of the ambient solar wind speed on the cutoff speed determination. A more detailed discussion of V_r is provided in Sect. 4.4.1. Furthermore, we propose improved methods to derive the cutoff speed and we present an approach to exclude acceleration sites from the data that may have an influence on the cutoff speed measurements. The final improvement of the original method that we introduce here is an error estimation that is based on a bootstrap Monte Carlo approach, similar to that utilized in Drews et al. (2012).

After these improvements, further systematic influences of external parameters on the result for the interstellar flow longitude from the PUI cutoff are investigated. As the PUI VDF and therefore the longitudinal transport of these ions, which should be minimized by concentrating on the PUI cutoff, is linked to the ambient IMF configuration, we test how the selection of IMF directions still affects the results of the analysis.

3. Data acquisition

PLASTIC is a time-of-flight mass spectrometer that measures energy-per-charge, time-of-flight, and residual energy from which the mass, charge, and energy of an incident ion can be calculated. Using this information one can extract the He^+ data of PLASTIC's solar wind section, as in Drews et al. (2010, 2012). Once an ion is identified, one can calculate the ion's speed in the spacecraft frame of reference from the energy-per-charge information, which makes it possible to derive the VDF of an ion species.

One great advantage of PLASTIC compared to other time-of-flight mass spectrometers (e.g., CTOF on SOHO or SWICS on ACE) is its position-sensitive detection system. The latitudinal angle of incidence is measured in the range of $-20°$ to $+20°$ in 32 steps with a deflection system, while the measurement of the azimuthal angle in the range of $-22.5°$ to $+22.5°$ in 32 steps is realized by evaluating the output of a resistive anode. This means that the velocity vector of the measured ion in the spacecraft frame, in this case $\boldsymbol{v}_{\rm He^+}$, can be fully reconstructed. This is true not only for PUIs, but also for the solar wind proton measurement, which yields the solar wind bulk velocity, $\boldsymbol{v}_{\rm sw}$, as a 3D vector. Thus, a transformation of the PUI velocity in

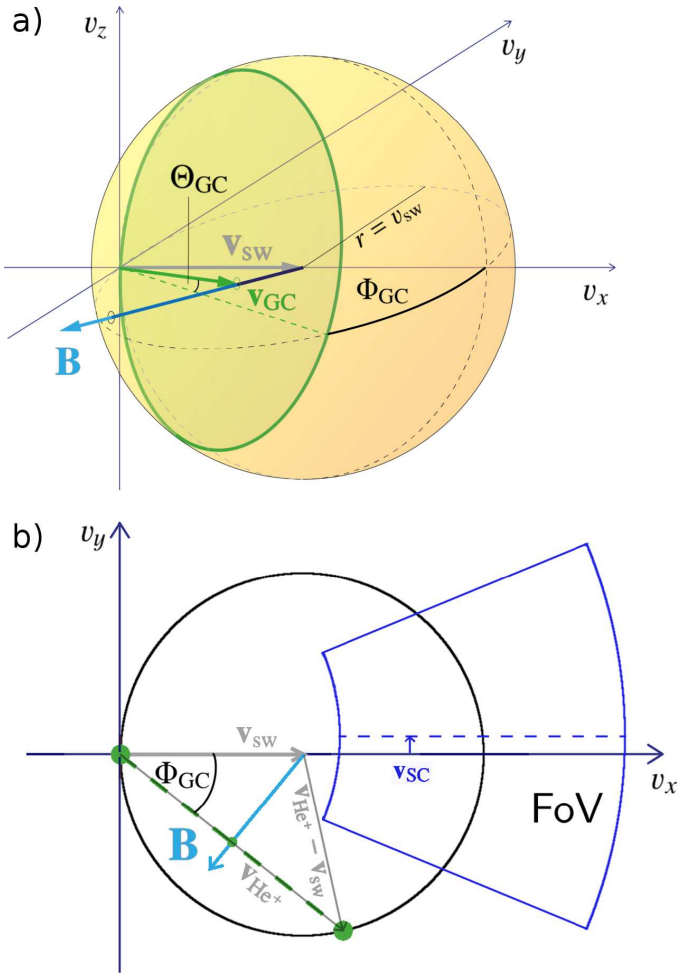

Fig. 1. Illustration of the ideal torus VDF of freshly injected PUIs. *Panel a*: 3D illustration, where v_x corresponds to the radial direction with respect to the Sun. PUIs at rest are injected into the solar wind plasma with a torus VDF that lies on a shell around the solar wind velocity. The radius of the shell equals the solar wind speed. The green line shows the velocity space trajectory of the PUIs around $\boldsymbol{B}$. The guiding center velocity of the torus, $\boldsymbol{v}_{GC}$, is shown with the green vector. Furthermore, the latitudinal angle, Θ_{GC}, of the guiding center velocity is illustrated. *Panel b*: 2D cut through the v_x-v_y plane of the configuration shown in *panel a*. For the intersection of the torus with the v_x-v_y plane, the velocity vectors in the spacecraft and solar wind frame of reference are shown. The area marked by the blue solid lines depicts PLASTIC's coverage in velocity space. It is not symmetrical about v_x, because of STEREO A's tangential eigen-velocity of 30 km s^{-1}. Freshly injected PUIs would obviously not be observed by PLASTIC under this IMF orientation. The angle Φ_{GC} corresponds to the azimuthal angle of the guiding center velocity.

the spacecraft frame, $\boldsymbol{v}_{He^+}$, into the solar wind frame, $\boldsymbol{v'}_{He^+}$, is possible.

Furthermore, we use the 1 min resolution IMF data provided by the IMPACT instrument suite (Acuña et al. 2008), a time resolution more than adequate for the PLASTIC data sets with a sensor cycle time of 5 min.

4. Analysis method

4.1. Physical motivation

In Fig. 2 an overview of the physical motivation of the approach to obtain the interstellar flow longitude, as introduced in Möbius et al. (2015), is given. Due to the Sun's gravitation, the interstellar neutral flow forms a characteristic structure around the Sun, which is symmetric about the interstellar flow direction (Fig. 2a). This symmetry is also found in the radial speed of the neutrals considering a fixed distance from the Sun (Fig. 2b). If these neutrals become ionized, their injection speed into the solar wind plasma depends on the relative motion of the parent neutral with respect to the solar wind, which is shown in Fig. 2c for the crescent ($\lambda \approx 255°$), the focusing cone ($\lambda \approx 75°$), and two intermediate locations ($\lambda \approx 165°$ and $\lambda \approx 345°$), illustrated with three different choices of the IMF orientation that keep the initial torus within the PLASTIC field of view (FoV). Consequently, the PUI VDF carries an imprint of the neutral's radial speed upon PUI injection, which manifests itself in the so-called PUI cutoff, which is discussed in the following section. We utilize this feature to determine the interstellar flow longitude.

4.2. Pickup ion cutoff

Due to their gyration about the IMF, PUIs are injected into the solar wind plasma with an anisotropic VDF that has the shape of a torus in velocity space. While traveling outward with the solar wind, the initial anisotropic VDF is gradually transformed into an isotropic VDF by pitch-angle scattering, which until recently was expected to be a rapid process. However, independent observations made by different spacecraft showed that in particular the He^+ VDF remains anisotropic for much longer than previously assumed (Oka et al. 2002; Drews et al. 2015; Taut et al. 2016).

For PUIs that are generated from neutrals at rest, this initial torus lies on a shell that is centered around the solar wind velocity and has a radius equal to the solar wind speed (Fig. 1). Consequently, these PUIs always move with solar wind speed in the solar wind frame of reference independent of the IMF orientation. For non-resting neutrals the injection speed, and therefore the radius of the shell, depends predominantly on the neutral's radial speed, as is pointed out in the previous section. Thus, this speed is directly related to the ecliptic longitude, where the ion is injected. In Fig. 2c three examples are shown corresponding to different ecliptic longitudes and IMF orientations.

Following the initial theory of PUI VDFs by Vasyliunas & Siscoe (1976), which implied a rapid isotropization by pitch-angle scattering and assumed no energy transfer between the solar wind and PUIs, no PUIs above the injection speed are expected to be observed. Hence, the so-called PUI cutoff would be a sharp edge of the VDF and it would be trivial to derive the injection speed. Instead, all PUI observations show a smooth decrease in count rate rather than a sharp edge. In the following, we call this decrease the PUI cutoff of the VDF.

There are two possible ways to explain the observation of PUIs above the injection speed. First, the most obvious explanation is that acceleration processes must act on the PUI VDF. Acceleration can occur locally due to compression regions or shocks, which is discussed in more detail in Sect. 4.3. Furthermore, even in the quiet solar wind a ubiquitous population of accelerated particles can be observed (see Fisk & Gloeckler 2012), which indicates that acceleration may continuously act on the PUI VDF.

Second, as can be seen from Fig. 1, the guiding center velocity of PUIs in the spacecraft frame is not necessarily equal to the solar wind velocity, especially at IMF orientations not at 90° to the solar wind. Hence, PUIs may be transported from the solar wind parcel where they were created at a given solar wind speed into another solar wind parcel with, for example, a slightly lower speed. In the solar wind frame of reference, these ions then appear to have a speed above the local injection speed because

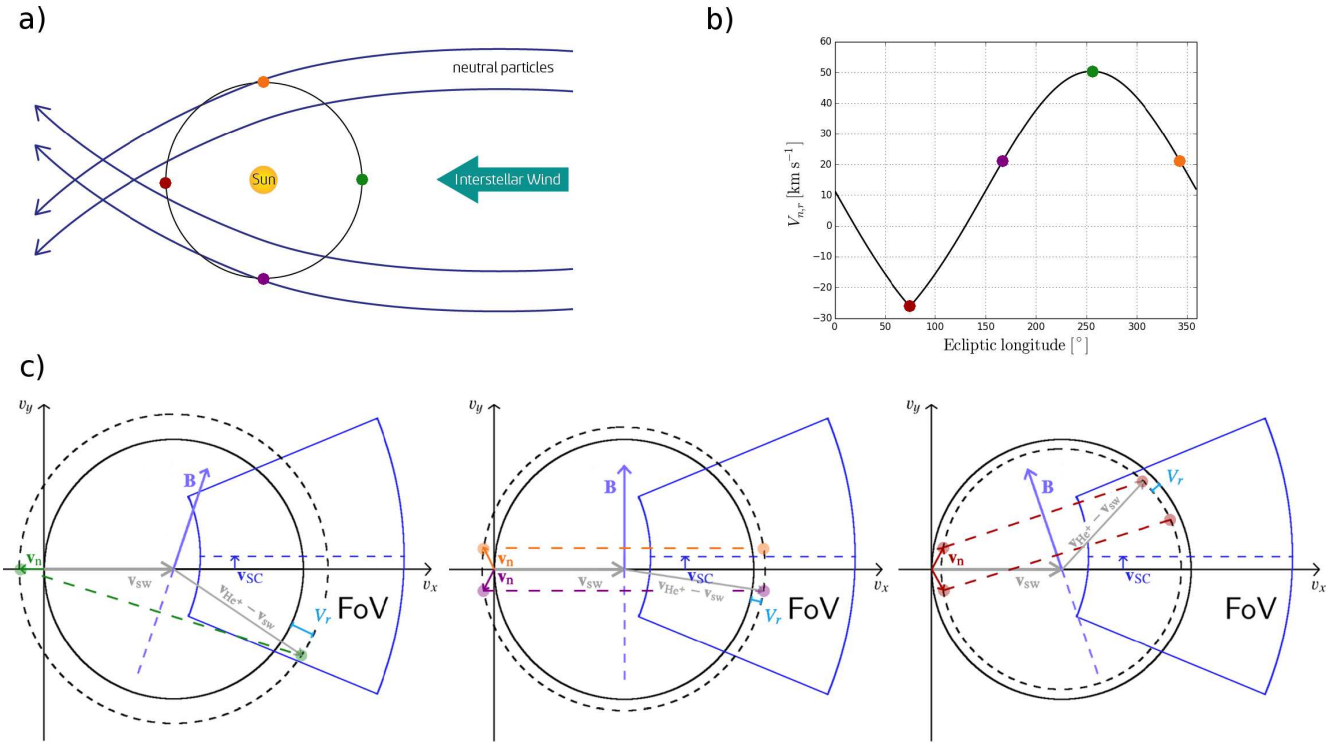

Fig. 2. *Panel a*: interstellar neutral flow in the ecliptic plane. Four sample trajectories are shown and four locations are marked by colored dots: green corresponds to the crescent ($\lambda \approx 255°$), dark red corresponds to the focusing cone ($\lambda \approx 75°$), and the orange and purple points correspond to ecliptic longitudes in between ($\lambda \approx 165°$ and $\lambda \approx 345°$). *Panel b*: Radial speed of the interstellar neutrals as a function of ecliptic longitude calculated from Eq. (5) with $\lambda_{\rm flow} = 75°$ and $v_{\rm ISN\infty} = 0.88$. The colored dots correspond to the ecliptic longitudes introduced in *panel a*. *Panel c*: 2D velocity space illustrations in the v_x-v_y plane for the PUI injection (Fig. 1). The velocity of the neutrals at each ecliptic longitude is shown as a colored vector. The bold circle illustrates the shell with radius v_{sw}, while the dashed circle depicts the shell on which the PUI torus lies that results from the non-zero radial speed of the parent neutral. For illustration purposes, the IMF orientation is chosen to lie within the ecliptic plane. The colored dashed lines illustrate the orientation of the torus VDF, the colored dots mark the points where the torus intersects with the v_x-v_y plane. *Left:* PUI injection in the crescent at an IMF orientation corresponding to $\Phi_{\rm GC} \approx -15°$. *Middle:* PUI injection between the crescent and focusing cone at an IMF orientation corresponding to $\Phi_{\rm GC} \approx 0°$. *Right:* PUI injection in the focusing cone at an IMF orientation corresponding to $\Phi_{\rm GC} \approx +15°$.

the PUI speed is always considered with respect to the solar wind speed (see Sect. 4.4.1).

Therefore, the measured PUI cutoff VDF is modulated by multiple processes, which makes it impossible to derive the precise injection speed from a measured PUI VDF. Fortunately, a relative cutoff speed shift as a function of ecliptic longitude is sufficient to find the interstellar flow longitude as the symmetry is still preserved for the relative speeds. For example, we can choose a characteristic point on the cutoff VDF which we define as the cutoff speed. This point must not necessarily correspond to the injection speed, but the offset of the injection speed to this characteristic point can be assumed to be constant, if the shape of the PUI cutoff VDF is constant at all ecliptic longitudes.

In any case, all processes modulating the PUI cutoff are stochastically distributed and, in particular, are not expected to show any dependence on ecliptic longitude. This means that when considering long-term data, these stochastic fluctuations of the PUI cutoff are expected to average out, resulting in a comparable shape of the cutoff for all ecliptic longitudes. If we assume that the PUI cutoff shape is approximately equal at all ecliptic longitudes, we can derive methods to find the relative cutoff speed, which are described in Sect. 4.4.2.

However, to justify this assumption we need to ensure that PLASTIC actually measures freshly injected ions. If the initial torus of freshly injected PUIs is not within the FoV of PLASTIC, only PUIs that already have undergone a scattering process are measured, which may completely alter the shape of the cutoff. In addition, it is very important for the determination of the interstellar flow longitude from the PUI cutoff that freshly injected PUIs are significantly less affected by possible PUI transport processes along the mean IMF.

To test whether the initial torus VDF of freshly injected PUIs is inside PLASTIC's aperture or not, the guiding center velocity, $\boldsymbol{v}_{\rm GC}$, of an ideal torus in the spacecraft frame is considered. We define the ideal torus as the theoretical velocity-space trajectory that an injected PUI with initial speed $V_n = 0$ would follow under a perfectly stable IMF configuration. Former PUI studies (e.g., Drews et al. 2015, 2016) and also Möbius et al. (2015) restrict the IMF data to orientations that lie ±20° within the ecliptic plane. Then it solely depends on the azimuthal angle of the IMF whether an ideal torus falls into PLASTIC's FoV or not. However, a huge amount of data is dismissed by this restriction, while there are IMF orientations possible, where the torus falls into the FoV without lying within the ecliptic plane.

The guiding center velocity of the ideal torus in the spacecraft frame, $\boldsymbol{v}_{\rm GC}$, can be derived by simple geometric arguments[1]:

$$\boldsymbol{v}_{\rm GC} = \boldsymbol{v}_{\rm sw} - \frac{B_x v_{\rm sw}}{|\boldsymbol{B}|^2}\boldsymbol{B}, \tag{1}$$

$$\Phi_{\rm GC} = \arctan 2(\boldsymbol{v}_{{\rm GC},y}, \boldsymbol{v}_{{\rm GC},x}), \tag{2}$$

[1] arctan 2 is the four-quadrant inverse tangent, which is sensitive to the signs of the arguments.

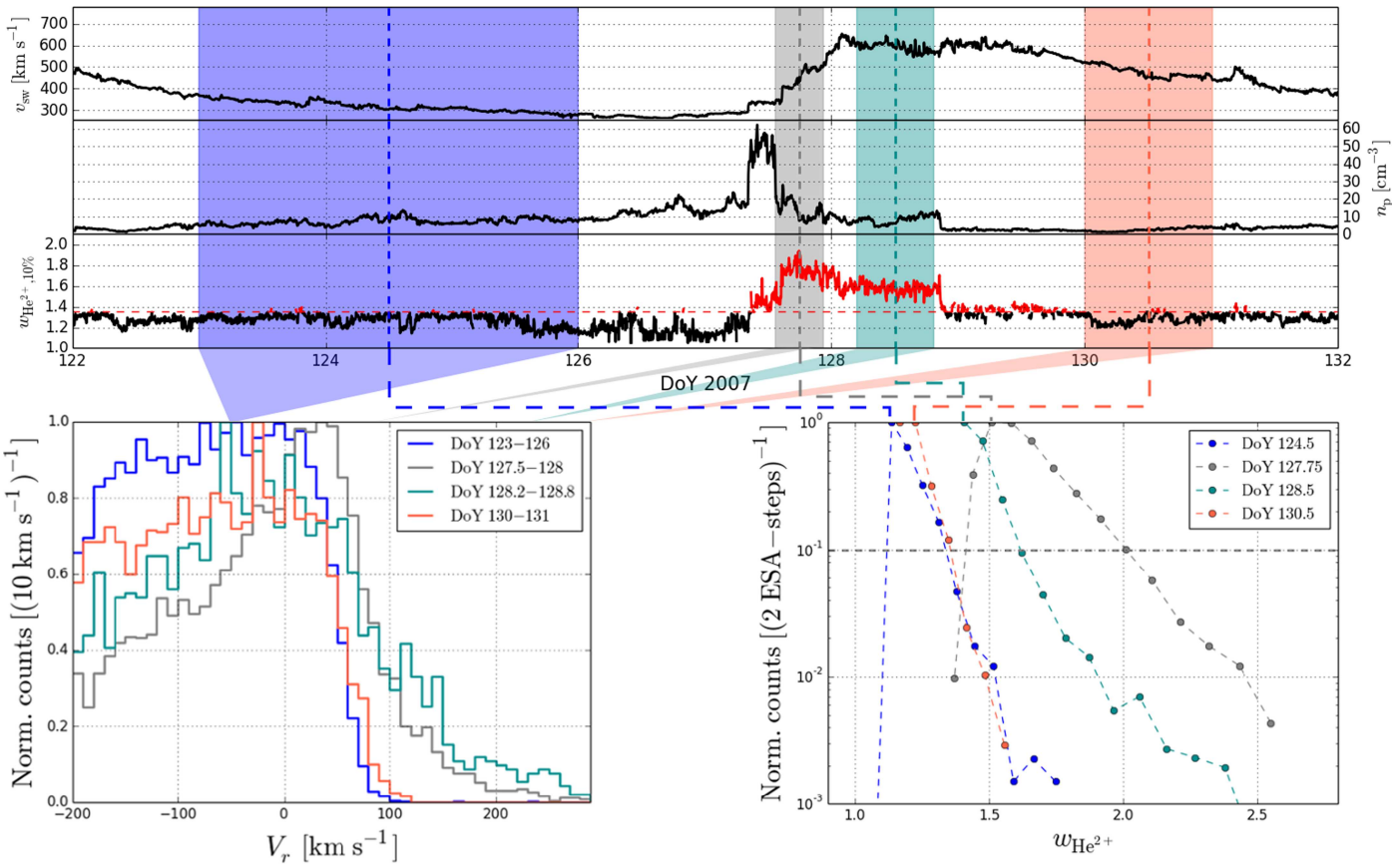

Fig. 3. *Upper panel*: solar wind speed, proton density, and the parameter $w_{He^{2+},10\%}$ derived from the He^{2+} VDF. Four time periods are marked that correspond to quiet solar wind (blue and red), compressed wind after the stream interface (gray), and compressed fast wind (cyan). Time periods that are displayed with the red solid line in the $w_{He^{2+},10\%}$ *panel* are excluded from our analysis. *Lower left panel*: He^+ count histograms measured in the marked time periods. *Lower right panel*: He^{2+} VDF measured by the sensor's main channel in one 5 min interval within the considered time periods.

$$\Theta_{GC} = \arcsin\left(\frac{\boldsymbol{v}_{GC,z}}{|\boldsymbol{v}_{GC}|}\right). \quad (3)$$

The azimuthal angle, Φ_{GC}, and the latitudinal angle, Θ_{GC}, correspond to the spherical coordinates of the vector. If $\boldsymbol{v}_{GC}$ is within PLASTIC's angular coverage, then also a slice of the gyrotropic torus VDF falls into its FoV. Thus, an ideal torus falls into PLASTIC's aperture if $-22.5° \leq \Phi_{GC} \leq 22.5°$ and $-20° \leq \Theta_{GC} \leq 20°$ neglecting STEREO A's eigen-velocity of $v_{SC} \approx 30$ km s^{-1} in the longitudinal direction. Only if $\boldsymbol{v}_{GC}$ fulfills both criteria are torus PUIs observed by PLASTIC. Due to v_{SC} the symmetry line of PLASTIC's velocity-space coverage is shifted with respect to the radial direction. This has the effect that the angular range of Φ_{GC}, where an ideal torus would be observed, is shifted by approximately +3° for very low solar wind speeds ($v_{sw} \approx 250$ km s^{-1}).

In Fig. 1 an example is shown for an arbitrary IMF orientation. In this example, the angular coordinates of $\boldsymbol{v}_{GC}$ are $\Theta_{GC} \approx +5°$ and $\Phi_{GC} \approx -40°$, which means that no torus PUIs are observed by PLASTIC under this IMF orientation.

4.3. Acceleration sites

As already indicated in Sect. 2, the observation of He^+ ions above the injection speed is evidence that acceleration processes may act on the He^+ VDF. Especially, shocks or compression regions like Stream Interaction Regions (SIRs) with a high level of turbulence (cf. Gloeckler et al. 1994; Schwadron et al. 1996) can efficiently accelerate PUIs above their injection speed. In turn, this means that the He^+ cutoff shape and location may be significantly altered by the increased abundance of accelerated PUIs, which would contradict the assumption that the PUI cutoff VDF is comparable at all ecliptic longitudes. More precisely, this may lead to a systematically higher cutoff speed at ecliptic longitudes where local acceleration sites are included in the data. These changes in the PUI cutoff will very likely bias the determination of the interstellar flow longitude, λ_{flow}.

In order to minimize the effect of time periods with a strong local acceleration on the cutoff measurements, we attempt to eliminate these occurrences. As a criterion for this task, we consider He^{2+} distributions also measured by PLASTIC. He^{2+} is of solar origin and thus does not vary systematically with ecliptic longitude. Also, its counting statistics are sufficient to yield a statistically significant representation of the VDF on a 5 min basis. It is reasonable to assume that acceleration processes in compressions act similarly on both ion species, He^+ and He^{2+} (e.g., Gloeckler 1999; Chotoo et al. 2000), or that at least signatures of acceleration processes that act on He^+ are visible in the He^{2+} VDF. Then, we can identify and eliminate time periods when the He^{2+} VDF is affected by acceleration processes.

Similar to the He^+ distributions, those of He^{2+} are derived from the raw PLASTIC pulse-height-analysis by the expected time-of-flight and residual energy signal at a given energy-per-charge step. For every He^{2+} count its speed relative to the solar wind speed, $w_{He^{2+}} = \frac{v_{He^{2+}}}{v_{sw}}$, in the spacecraft frame is calculated.

The solar wind section of PLASTIC has another feature that we utilize here. The energy-per-charge values are stepped through from high to low values. If the particle flux exceeds a certain limit when the energy steps approach the He^{2+} bulk flow energy, the sensor switches to the so-called small channel, which reduces its geometric factor. Because the channel switch occurs at a fixed count rate we can treat this threshold as a reference flux. In the following, we use the normalized speed of He^{2+} ions $w_{He^{2+},10\%}$ where the He^{2+} rate exceeds 10% of the channel switch threshold value as a condition for effective acceleration of He^{2+} ions and thus by inference also of He^{+} PUIs.

We motivate the choice of our condition for interplanetary acceleration with the display of the He^{+} and He^{2+} VDFs over the course of an SIR in Fig. 3. The spectra are taken during four time intervals, which are marked in blue, gray, cyan, and red. In the solar wind speed and density data one can clearly identify the SIR at approximately DoY 127 – 129 by the strong increase in density, which is subsequently followed by a sudden drop and then an increase in solar wind speed (see Jian et al. 2006). The blue and red periods correspond to comparatively undisturbed solar wind before and after the SIR, respectively. The time period marked in gray corresponds to turbulent wind right after the spacecraft passed the stream interface, which can be identified by the sudden drop in proton density. The time period marked in cyan already has a slight negative gradient in solar wind speed. Nevertheless, the proton density (and the He^{2+} spectra) suggest that compressed fast solar wind is observed.

In the lower left panel the He^{+} spectra measured in the four time periods are displayed. In the quiet solar wind, a sharp cutoff is observed that matches the expected injection speed of $V_r \approx 50$ km s^{-1} as the time period can be assigned to a position of STEREO A close to the interstellar upwind direction in ecliptic longitude ($\lambda \approx 230°$). The other two spectra appear to be shifted to higher speeds and show a distinct tail extending to higher speeds, which indicates the acceleration of He^{+} ions. In the lower right panel of Fig. 3 the He^{2+} spectra taken in the main channel are displayed for one 5 min interval within each considered time period. Obviously, the channel switch and thus the 10% value of the threshold rate occurs at a higher $w_{He^{2+}}$ in the time periods with compressed solar wind where PUI acceleration is observed when compared with quiet solar wind. Furthermore, the count rate decrease as a function of $w_{He^{2+}}$ is steeper in the quiet solar wind than right after the stream interface. Both effects lead to low $w_{He^{2+},10\%}$ values in the quiet wind and enhanced $w_{He^{2+},10\%}$ values in compressed wind and thus supposedly in acceleration sites. The increased threshold speed $w_{He^{2+},10\%}$ can be traced to three different causes or a combination of them: 1) the acceleration efficiency is high, which expresses itself as a hard spectrum in $w_{He^{2+}}$ (gray spectrum); 2) a large fraction of the He^{2+} distribution is injected into acceleration; or 3) the density of solar wind He^{2+} is very high, e.g., due to a solar wind compression. Both 2) and 3) would push the He^{2+} spectrum to higher $w_{He^{2+},10\%}$ values (as in the green spectrum). All three effects are expected to occur in conjunction with solar wind compression regions and thus also to lead to effective He^{+} acceleration.

Figure 4 shows a composite 2D histogram of the normalized He^{+} PUI counts as a function of V_r versus $w_{He^{2+},10\%}$ accumulated for time intervals in the PUI crescent region ($230° \leq \lambda \leq 280°$). At these ecliptic longitudes the PUI injection speed is almost constant with variations $\lesssim$5 km s^{-1}. When a He^{2+} spectrum is measured that results in $w_{He^{2+},10\%} > 1.35$, the He^{+} distributions appear to extend to substantially higher speeds. This observation seems to indicate that under this condition the assumption of a cutoff VDF with comparable shape independent of ecliptic longitude is violated. To ensure that the cutoff VDF has a comparable shape and to minimize this effect on the λ_{flow} determination, we filter the entire data set by requiring $w_{He^{2+},10\%} \leq 1.35$.

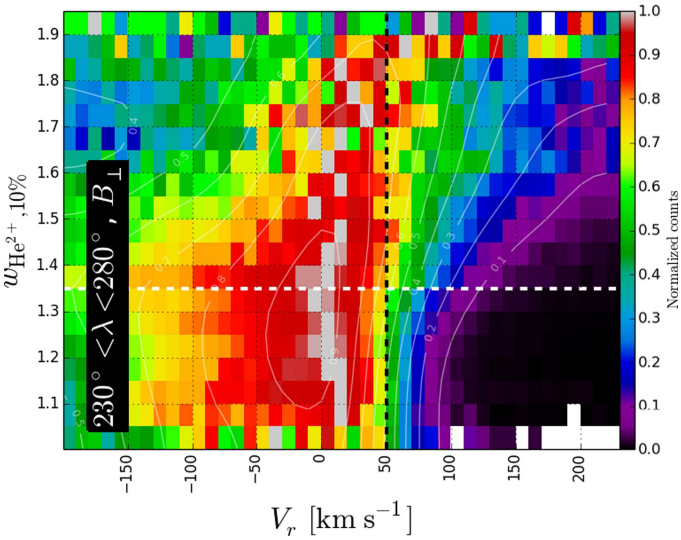

Fig. 4. Two-dimensional histogram of He^{+} PUI counts in the crescent range of ecliptic longitude ($230° \leq \lambda \leq 280°$) depending on V_r and $w_{He^{2+},10\%}$. Only IMF configurations where the torus VDF of freshly injected PUIs is measured by PLASTIC's aperture are considered by selecting $-15° \leq \Theta_{GC} \leq 15°$ and $-15° \leq \Phi_{GC} \leq 15°$. The counts per bin are normalized to the maximum of each $w_{He^{2+},10\%}$ bin. The nominal cutoff in this range of ecliptic longitude is indicated by the vertical black dashed line. Above $w_{He^{2+},10\%} = 1.35$ (white dashed line) the cutoff smears out to higher speeds, which indicates that acceleration processes must have acted on the He^{+} VDF.

Of course, the method we use to exclude acceleration sites is an empirical approach that is not based on an evaluation of the details of the physical processes that lead to tails or a shift of the PUI VDF to higher speeds. However, as can be seen from the example in Fig. 3, all three effects that can lead to a local appearance of accelerated He^{2+} and thus per inference of He^{+} PUIs seem to be captured by this method. A more detailed investigation of these observations and their implications goes beyond the scope of this work and may be the subject of an independent follow-up investigation. Figure 4 shows that our empirical approach to use the value $w_{He^{2+}}$ where the He^{2+} distribution exceeds a threshold flux serves as a good indicator for acceleration of He^{+} PUIs.

4.4. Determining the pickup ion cutoff speed

The concept we use to determine λ_{flow} from the variation of the cutoff speed is identical to that of the method described in Möbius et al. (2015). First, the data is filtered for suitable IMF configurations (Sect. 2), and sites of strong local acceleration are excluded (Sect. 4.3) to ensure that the shape of the PUI cutoff is approximately the same. Then, the data is split into bins of ecliptic longitude, for which a histogram of the He^{+} counts as a function of V_r is created. The speed V_r of each He^{+} count is calculated from the He^{+} speed in the solar wind frame and the solar wind speed. It is introduced more explicitly in the following section. For each histogram, the cutoff speed is determined,

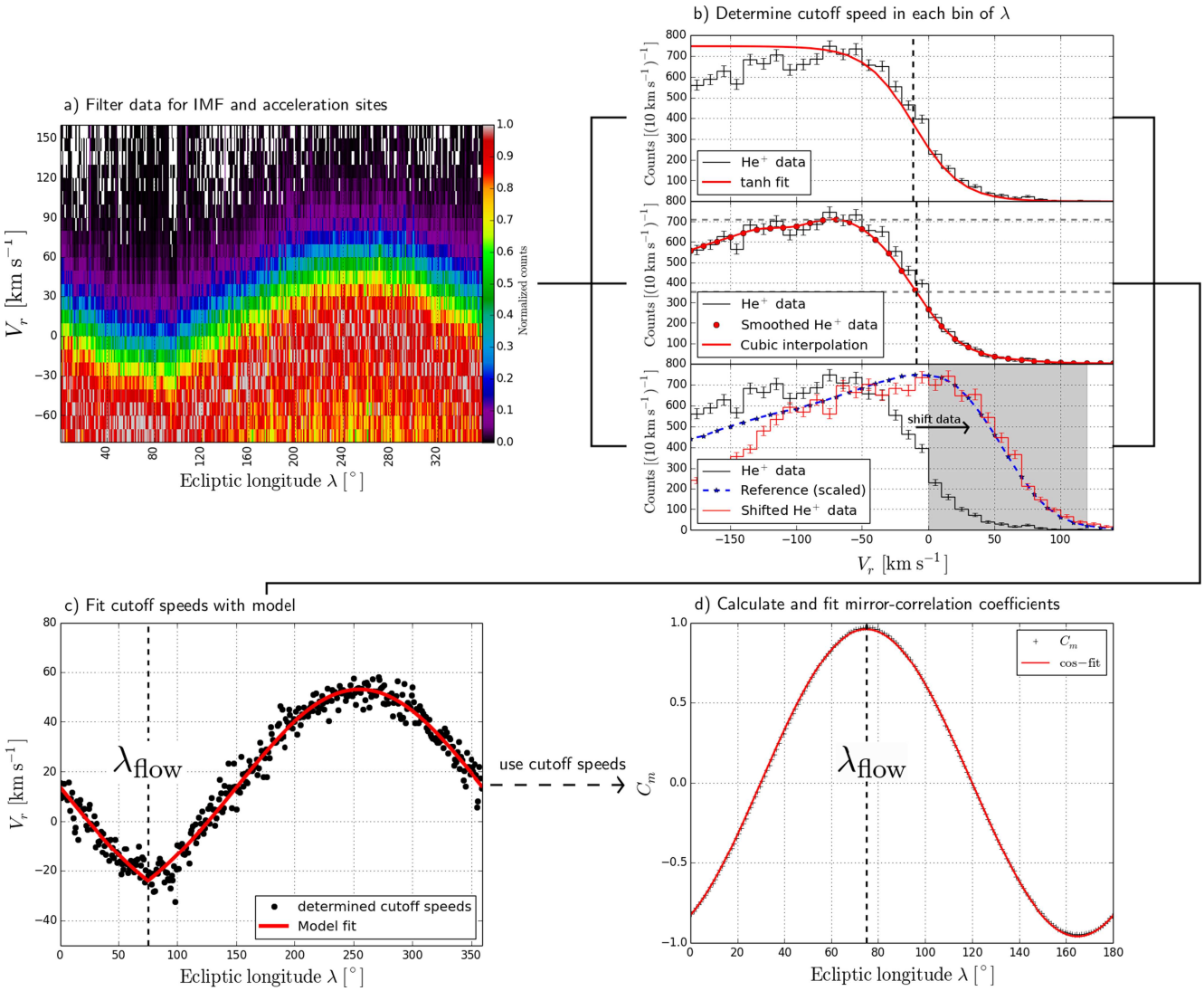

Fig. 5. *Panel a*: two-dimensional histogram of He^+ counts as a function of ecliptic longitude, λ, and V_r. The data have been filtered for IMF orientation according to $-15° \leq \Theta_{GC} \leq 15°$ and $-15° \leq \Phi_{GC} \leq 15°$ (see Sects. 3 and 6), and acceleration sites by requiring $w_{He^{2+},10\%} \leq 1.35$ (see Sect. 4.3). The counts per bin are normalized to the maximum of each λ bin. *Panel b*: demonstration of the three cutoff determination techniques performed on the example of bin $\lambda = 100°$. The *upper panel* shows the tanh-fit as used in Möbius et al. (2015), the *middle panel* shows the 50% threshold method, and the *lower panel* illustrates the maximization of the correlation coefficient with a reference curve. *Panel c*: resulting cutoff speeds from the threshold method as a function of λ. The interstellar flow longitude is determined by fitting Eq. (5) to the results. *Panel d*: mirror-correlation coefficients for every bin of λ calculated from the cutoff speeds. The interstellar flow longitude is determined by fitting a cos-function to the resulting correlation coefficients.

and λ_{flow} is derived from the variation of these speeds with longitude. However, we introduce improvements in each of these steps that are described in the following sections. An overview of the analysis including an example for each step of the analysis is illustrated in Fig. 5.

4.4.1. Frame of reference

Due to the pickup process, the speed of PUIs is always related to the ambient solar wind speed. This is why the PUI VDF has commonly been considered in terms of the PUI speed normalized to the solar wind speed, $w_{He^+} = \frac{v_{He^+}}{v_{sw}}$, which is typically considered in the spacecraft frame of reference (see Kallenbach et al. 2000). However, in this frame the speed of a freshly injected ion is not constant due to the gyration about the IMF. For example, the speed of a PUI created from a neutral at rest alternates between 0 and the maximum speed of $2v_{sw}$ for an IMF configuration perpendicular to the solar wind. Furthermore, the maximum speed of a freshly injected PUI depends on the IMF orientation. Only the velocity component perpendicular to the IMF of the relative motion of the former neutral and the solar wind is crucial for the gyration speed. For example, in Fig. 1 a non-perpendicular IMF orientation is illustrated, where obviously the freshly injected torus PUIs reach a substantially lower maximum speed in the spacecraft frame than $2v_{sw}$. Considering the cutoff VDF in this frame, it is clear that it is severely influenced by the IMF orientation.

As already mentioned in Sect. 2, transforming the PUI speed into the solar wind frame of reference has the advantage that for a given solar wind speed, the injection speed of freshly injected PUIs is conserved for a given ecliptic longitude under any IMF orientation. Therefore, in Drews et al. (2015), the data product $w'_{He^+} = \frac{v'_{He^+}}{v_{sw}}$ has been introduced. This data product has also been utilized in Möbius et al. (2015) to determine the cutoff speed. However, using this quantity introduces an implicit dependence

of the variation of the cutoff speed with longitude on the solar wind speed through the normalization in w'_{He^+}. This effect can be demonstrated by considering a simplified situation: for ecliptic longitudes close to the interstellar upwind direction, the interstellar neutrals stream anti-parallel to the solar wind with a speed $V_n \approx 50$ km s^{-1} with respect to the Sun. Therefore, their injection speed in the solar wind frame equals the relative speed between the neutrals and the solar wind. Assuming a solar wind speed, $v_{sw,1} = 300$ km s^{-1}, the injection speed would be $v_{inj,1} = 350$ km s^{-1}; at a higher solar wind speed of $v_{sw,1} = 600$ km s^{-1}, the injection speed would be $v_{inj,1} = 650$ km s^{-1}. In terms of w_{He^+}, these injection speeds correspond to $w_{He^+,1} = 1.17$ and $w_{He^+,2} = 1.08$ for the same ecliptic longitude. Thus, the cutoff speed in terms of w_{He^+} shows a clear dependence on solar wind speed. Because the neutral particle speed is constant at a given ecliptic longitude and does not depend on the solar wind speed, it is not advisable to use the normalized PUI velocity for the evaluation of the interstellar neutral gas flow.

Therefore, we chose to consider the cutoff in terms of V_r:

$$V_r = v'_{He^+} - v_{sw}. \quad (4)$$

The first term, $v'_{He^+} = |\boldsymbol{v}_{He^+} - \boldsymbol{v}_{sw}|$, corresponds to the PUI speed in the solar wind frame of reference (see Fig. 1). PLASTIC is able to measure this speed because information about the ion incident angle is provided by the azimuthal deflection steps and the latitudinal position bins (see Sect. 3). Thus, V_r is the difference between the PUI speed and the ideal torus shell, which is also illustrated in Fig. 2c. Throughout this paper, we use He^+ histograms in terms of V_r with a bin-width of 10 km s^{-1}.

4.4.2. Techniques for determining cutoff speed

In Möbius et al. (2015) a tanh-function is utilized to fit the cutoff in the He^+ spectra in every ecliptic longitude bin. The point of inflection of the tanh-function is then used as the cutoff speed. This method is illustrated in the upper panel of Fig. 5b. It yields reasonable results for the cutoff speeds if the He^+ counting statistics are sufficiently high in the considered bin of ecliptic longitude.

If the He^+ counting statistics in the ecliptic longitude bin is very low (maximum of ~10 counts bin^{-1} in the V_r histogram) the counts per bin are strongly fluctuating due to statistical noise. In this case, the tanh-fit of the cutoff is likely to yield highly variable results for the cutoff speeds that deviate significantly from the expected values.

Therefore, we developed another method to determine the cutoff speed that is independent of a functional fit to the histogram. Instead, we smooth the histogram with a 3–V_r–bin weighted running average, where the weights are calculated from a normal distribution centered on the considered bin with a width of 3 bins. Additionally, a cubic interpolation is calculated for the smoothed data. Using this interpolation we define the cutoff speed as the speed where this interpolation matches 50% of the maximum of the smoothed data. An example of this method for a given bin of λ is displayed in the middle panel of Fig. 5b. The results of this procedure are expected to be similar to those returned by the fit method as the tanh-function also has its point of inflection at 50% of its maximum.

We also developed a third option to determine the cutoff speed that is independent from the other two methods to check how the cutoff determination method affects the result for the interstellar flow longitude. This method relies on the maximization of the correlation between the measured distributions and a reference curve. The reference curve is derived from data accumulated over a range of ecliptic longitude of $250° < \lambda < 260°$ as no significant changes of the nominal cutoff speed are expected in this range. Furthermore, the reference curve is smoothed with a three-bin running-average. In each bin of ecliptic longitude, the measured spectra are now shifted in V_r such that the correlation between the spectrum and the reference curve reaches a maximum. This means that in order to find the offset ΔV_r, we need to add to the measured spectra to obtain a maximum correlation coefficient calculated with the reference curve. As we are only interested in the part of the distribution where the cutoff is located, we focus on the range 0 km s^{-1}< V_r <120 km s^{-1} of the reference curve. In the lower panel of Fig. 5b, a demonstration of this method is given. The shift, ΔV_r, that is applied to the data to reach the maximum correlation in one bin of ecliptic longitude is taken as the relative cutoff value. As we are comparing each cutoff VDF with the reference curve taken from the crescent, we expect the highest shift ΔV_r in the focusing cone and $\Delta V_r \approx 0$ km s^{-1} in the crescent. This means that the sign of the ΔV_r needs to be flipped to obtain the same curve shape of cutoff speed versus ecliptic longitude as the other two methods obtain, and which is shown in Fig. 5c. However, the sign of ΔV_r is irrelevant with respect to the λ_{flow} determination methods introduced in the next section.

In Sect. 6.1 we apply all three methods to the same data set and compare the results obtained for the interstellar flow longitude.

4.5. Determining the interstellar flow longitude

In Möbius et al. (2015) the authors propose that a precise method for determining the interstellar flow longitude, λ_{flow}, from the PUI cutoff is to calculate a mirror-correlation coefficient, C_m, for every bin of ecliptic longitude and then fit this data with a cos-function with variable amplitude and phase. The resulting value for the phase-parameter corresponds to the position of the focusing cone or crescent, respectively. An example of this method is shown in Fig. 5d. The main advantage of this method is that it is completely independent from any model of the radial neutral particle speed as the only assumption is that it is symmetric about the flow direction. The disadvantage is that it neglects that the STEREO A orbit is not a perfect circle, which of course affects the symmetry of the measured cutoff speeds and introduces a systematic error on the order of $\Delta\lambda_{flow} \approx 0.1°$, which is discussed in Möbius et al. (2015).

In Möbius et al. (2015) an analytical model for the radial neutral particle speed at 1 AU is also given,

$$v_{n,r}^2 = 2 + v_{ISN\infty}^2 - (1 - \cos\lambda) - \Big[v_{ISN\infty}^2 \sin^2\lambda + v_{ISN\infty} \sin|\lambda| \sqrt{v_{ISN\infty}^2 \sin^2\lambda + 4(1 - \cos\lambda)} \Big] / 2, \quad (5)$$

where $v_{n,r} = \frac{V_{n,r}}{V_E}$ and $v_{ISN\infty} = \frac{V_{ISN\infty}}{V_E}$ is the neutral particle speed at the observer and infinity, respectively, normalized to $V_E = \sqrt{\frac{GM_S}{R_E}}$ with the gravitational constant, G; solar mass, M_S; and Sun–Earth distance, $R_E = 1$ AU. The interstellar flow longitude, λ_{flow}, is connected to λ via $\lambda = \lambda_{Obs} - \lambda_{flow} - 180°$. We note that this equation has been derived under the assumption that the orbital plane of the neutrals is equivalent to the ecliptic plane, which means that the latitudinal tilt of the interstellar neutral flow has been neglected.

Using this equation, one can also perform a three-parameter least-squares fit of the cutoff speed data with λ_{flow}, $V_{\mathrm{ISN}\infty}$, and an offset as free parameters. By using the known relation of ecliptic longitude and solar distance of STEREO A, it is easy to consider the STEREO A orbit in this fit by renormalizing the parameters. The model matches the data reasonably, which can be seen in the example in Fig. 5c.

We use both of these methods for the determination of the interstellar flow longitude from the He^+ cutoff values and compare the results in Sect. 6.1.

5. Error estimation

Concerning the estimated error that our analysis yields for λ_{flow}, we distinguish between two different errors related to their different sources. On the one hand, our analysis has a statistical error due to the limited He^+ counts. On the other hand, varying solar wind conditions that slightly influence the determined cutoff speeds may lead to a systematic but stochastically distributed error. Both errors can be estimated using Monte Carlo techniques.

Generally, count rates such as those in the V_r histograms for every bin of ecliptic longitude follow Poisson statistics. Thus, we estimate the statistical error by adding Poissonian noise according to the counting statistics for each bin to the V_r histograms and repeating the analysis $N = 1000$ times using data sets modified in this way. The standard deviation of the results for λ_{flow} serves as our estimate for the purely statistical error.

The estimate of the stochastic error is a little more involved. Here, we exploit that our data consist of seven STEREO A orbits. Thus, there are seven independent and decoupled measurements of the cutoff under different solar wind conditions. By discarding two orbits of data each time, we get 21 different combinations of five out of seven orbits with sufficient statistics that we can utilize to estimate the error of our analysis that is introduced by the slight variation of the cutoff due to varying solar wind conditions. This method is closely related to the error estimation for λ_{flow} utilized by Drews et al. (2012). In the approach applied in this work, variations of the interplanetary conditions introduce stochastically distributed fluctuations in the PUI flux, which is utilized to determine the location of the focusing cone and crescent. Consequently, we derive the cutoff in every bin of ecliptic longitude for all 21 combinations of 5 orbits. Afterwards, we determine λ_{flow} $N = 1000$ times by randomly choosing one of these 21 results in every bin of ecliptic longitude. The standard deviation of the results for λ_{flow} serves as our total error estimate that includes both error sources.

6. Results

In the previous sections, we presented approaches to eliminate systematic effects that may influence the result for the interstellar flow longitude, λ_{flow}, derived from the PUI cutoff and a new approach for estimating the error of the obtained λ_{flow} value. Now we apply this modified analysis to STEREO A/PLASTIC He^+ PUI observations from 2007 through 2014.

6.1. Updated results for the interstellar flow longitude

First, we compare how the different methods for determining cutoff and the two different options used to derive the interstellar flow longitude from the cutoff speeds affect the results. For this, we take data filtered for IMF configurations where the PUI torus is supposedly covered by PLASTIC's velocity space coverage. To ensure that the torus is inside PLASTIC's aperture in the latitudinal and longitudinal direction we restrict the data to IMFs where $-15° \leq \Theta_{\mathrm{GC}} \leq 15°$ and $-15° \leq \Phi_{\mathrm{GC}} \leq 15°$, respectively. The bin width of ecliptic longitude is chosen to be $\Delta\lambda = 1°$. To demonstrate the effect of acceleration sites on the analysis, we compare how the filter for $w_{\mathrm{He}^{2+},10\%} \leq 1.35$ influences the obtained values for λ_{flow} and its errors. The results are summarized in Table 1.

First of all, the result that the observed curve of the cutoff speeds (Fig. 5c) fits the predicted behavior of the injection speed (Fig. 2b) shows that the assumption that we can relate the PUI cutoff speed to the injection speed is justified. Furthermore, the stochastic errors of all methods are significantly smaller than one bin width and the very high correlation coefficients of the mirror-correlation imply a high level of symmetry.

Considering the results from the data set, which has not been filtered for acceleration sites, one can see that the results derived from the different cutoff determination techniques deviate significantly from each other. In particular, the λ_{flow} values derived from the tanh-fit and the 50% threshold technique do not agree within their mutual stochastic errors. Apparently, different cutoff determination techniques have a different sensitivity to the impact of acceleration sites. The systematic errors that are introduced, which are stochastically distributed over ecliptic longitude, lead to the differences in the results for λ_{flow}.

This is not the case for the data set in which acceleration sites have been excluded. The 50% threshold method shows a small deviation ($\Delta\lambda_{\mathrm{flow}} \approx 0.25°$) from the other two methods that obtain very similar results ($\Delta\lambda_{\mathrm{flow}} \approx 0.04°$). However, all values agree within their mutual uncertainties, both statistical and stochastic. Furthermore, a decrease of the stochastic errors is observed when filtering the data for acceleration sites. This is also supported by the increase in the maximum mirror-correlation coefficient, which implies that an enhanced symmetry of the cutoff speeds is obtained. These results support the conclusion that it is necessary to exclude acceleration sites from the data. Consequently, we only discuss the results obtained from the filtered data in the following.

All results for λ_{flow} from the filtered data show a significant deviation of $\Delta\lambda_{\mathrm{flow}} \approx -1°$ from the value presented in Möbius et al. (2016a) : $\lambda_{\mathrm{flow}} = 76.19° \pm 0.04°$. The statistical error is in all cases slightly larger than the value of $\sigma_{\mathrm{stat.}} = 0.15°$ estimated in Möbius et al. (2016b). Furthermore, the tanh-fit method seems to be most affected by statistical fluctations, while the maximum correlation method is the most stable with respect to statistics. Interestingly, this trend is inverted for the stochastic error, which is introduced by the variability of solar wind conditions. It is about a factor of two larger than the statistical error. The uncertainty for λ_{flow} given in Möbius et al. (2016a) was highly underestimated as the stochastic error derived with our approach is about one order of magnitude larger. However, Möbius et al. (2015, 2016a) explicitly noted that their error estimate was solely based on statistical considerations and that systematic errors would likely be larger and still needed to be studied. In any case, the difference between the obtained errors of the different cutoff determination techniques is on the order of 10%.

While inside the stochastic uncertainties, there seems to be a consistent difference between the interstellar flow longitude determined from the mirror-correlation and the direct fit with Eq. (5). The cos-fit of the mirror-correlation coefficients obtained λ_{flow} values that are $\Delta\lambda_{\mathrm{flow}} \approx 0.2°$ lower than those derived from the fit of Eq. (5) to the cutoff speeds. To

Table 1. Results for the interstellar flow longitude, $\lambda_{\rm flow}$, from the He^+ PUI cutoff derived from three different methods to determine cutoff and two different ways to determine $\lambda_{\rm flow}$ from the cutoff speeds.

Method	Mirror-correlation				Model-fit		
	$\lambda_{\rm flow}$ [°]	max(C_m)	$\sigma_{\rm stat.}$ [°]	$\sigma_{\rm stoch.}$ [°]	$\lambda_{\rm flow}$ [°]	$\sigma_{\rm stat.}$ [°]	$\sigma_{\rm stoch.}$ [°]
Without $w_{He^{2+},10\%}$ filter							
tanh-fit	75.33	0.965	0.27	0.45	75.62	0.24	0.45
50% threshold	76.11	0.954	0.18	0.54	76.39	0.16	0.50
max. correlation	75.78	0.968	0.17	0.45	75.98	0.15	0.43
With $w_{He^{2+},10\%}$ filter							
tanh-fit	75.18	0.975	0.23	0.35	75.41	0.22	0.34
50% threshold	74.88	0.971	0.20	0.36	75.17	0.18	0.35
max. correlation	75.15	0.974	0.18	0.41	75.34	0.16	0.39

Notes. The maximum of the mirror-correlation coefficients, max(C_m), and the errors, $\sigma_{\rm stat.}$ and $\sigma_{\rm stoch.}$ discussed in Sect. 5 are displayed. The IMF filter was set to $-15° \leq \Phi_{\rm GC} \leq 15°$ and $-15° \leq \Theta_{\rm GC} \leq 15°$. For the results displayed in the lower rows, we required $w_{He^{2+},10\%} \leq 1.35$ in the data selection to exclude acceleration sites.

some extent, this may be connected to the non-circular orbit of STEREO A, which is considered in Eq. (5) and not in the mirror-correlation approach, but it is likely not the entire reason because the estimated difference for the ellipticity is smaller. Furthermore, comparing the statistical and stochastic errors estimated for the two different $\lambda_{\rm flow}$ determination methods, it can be seen that both produce comparable uncertainties.

6.2. Influence of $\Phi_{\rm GC}$ on $\lambda_{\rm flow}$ results

The enhanced data quality that is established by the improvements of the method makes it possible to study further systematic influences on the results for $\lambda_{\rm flow}$. A key parameter that affects the PUI VDF, and therefore the PUI transport, is the IMF orientation. As we are only interested in the interstellar flow longitude, the parameter $\Phi_{\rm GC}$ is crucial as a latitudinal transport effect or the latitudinal orientation of the torus is not supposed to affect the derived interstellar flow longitude.

Thus, we perform the analysis with data sets filtered for different IMF configurations and focus on the parameter $\Phi_{\rm GC}$. We require again that $-15° < \Theta_{\rm GC} < 15°$ to ensure that the ideal torus falls into PLASTIC's FoV in the range of $-22.5° \lesssim \Phi_{\rm GC} \lesssim 22.5°$. Furthermore, we still exclude sites with enhanced local acceleration signatures by filtering the data for $w_{He^{2+},10\%} \leq 1.35$. As we want to explore the entire range of possible $\Phi_{\rm GC}$ angles, this means that the ideal torus is not necessarily in PLASTIC's FoV, in particular in the range $|\Phi_{\rm GC}| \gtrsim 22.5°$. For the cutoff determination method we chose the 50% threshold approach as this method copes best with low statistics, which can occur due to the narrow selection of IMF data. For the determination of $\lambda_{\rm flow}$ the direct model fit was chosen, because of the smaller uncertainties and the elliptical orbit of STEREO A which is considered in the model.

In Fig. 6 one can see the results for $\lambda_{\rm flow}$ over the $\Phi_{\rm GC}$ range. It is apparent that for IMF configurations where an ideal torus would be measured by PLASTIC's aperture (red shaded area) the result for $\lambda_{\rm flow}$ depends approximately linearly on the selected $\Phi_{\rm GC}$ range. This trend seems to continue for configurations where an ideal torus would be just outside PLASTIC's aperture, which is probably related to the non-zero width of a real torus VDF. At magnetic field configurations where the torus is clearly outside of PLASTIC's aperture ($|\Phi_{\rm GC}| \gtrsim 40°$) no correlation between the IMF configuration and the result for $\lambda_{\rm flow}$ is observed, although these data points have comparatively large

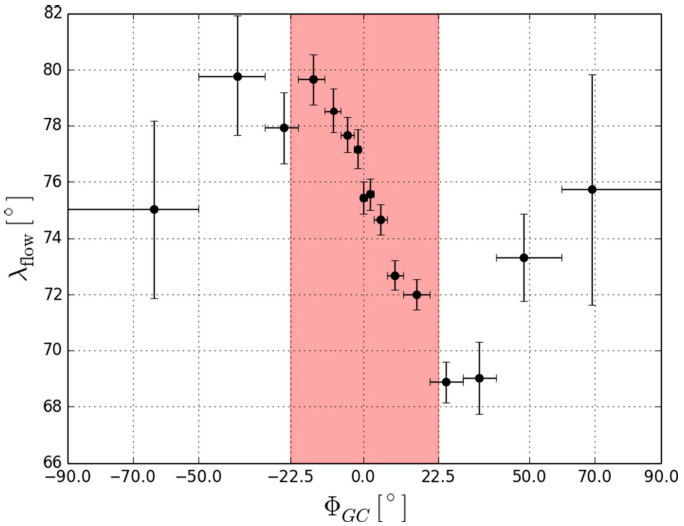

Fig. 6. Results of $\lambda_{\rm flow}$ for different selections of IMF orientations in terms of $\Phi_{\rm GC}$. Due to the small sample size, especially in the $|\Phi_{\rm GC}| \gtrsim 40°$ region, a comparatively coarse resolution in ecliptic longitude of $\Delta\lambda = 4°$ was chosen for the analysis. The error of $\lambda_{\rm flow}$ corresponds to the stochastic error, while the errorbars in $\Phi_{\rm GC}$ illustrate the selected $\Phi_{\rm GC}$ range. The data points are displayed at the mean $\Phi_{\rm GC}$ value for each range. The red area corresponds to the values where an ideal torus would be detected by PLASTIC neglecting STEREO A's eigen-velocity.

error bars. We also performed this analysis using the other cutoff determination methods, which produced similar results and in particular the same clear trend that can be seen in Fig. 6.

Comparing these results to the values determined from a broad range of IMF data that are displayed in Table 1, one can see that these values are slightly lower than the intersection of the curve in Fig. 6 with $\Phi_{\rm GC} = 0°$, but within the stochastic uncertainties. This difference may be caused by the fact that IMF angles with $\Phi_{\rm GC} > 0°$ occur more frequently than IMF angles with $\Phi_{\rm GC} < 0°$, because angles with $\Phi_{\rm GC} > 0°$ are closer to the Parker angle which corresponds to the mean IMF.

7. Discussion

As already mentioned in the previous section, the results listed in Table 1 deviate considerably from the result presented in Möbius et al. (2016a), $\lambda_{\rm flow} = 76.19° \pm 0.04°$. This supports the

hypothesis that systematic influences like the dependence of the cutoff speed on the solar wind speed, which we eliminated by deriving the cutoff in terms of V_r instead of w_{sw}, or the presence of acceleration sites may have a strong impact on the result for λ_{flow}, which cannot be neglected. Our error estimate, which now includes contributions from stochastically distributed variations in the interplanetary conditions, is about one order of magnitude higher for our results than presented in Möbius et al. (2015, 2016a), which is solely the pure fit error of the cos-fit to the mirror-correlation coefficients. The errors presented in Table 1 are derived from a totally different approach. On the one hand, it takes into account the limited counting statistics; on the other hand, the varying solar wind conditions that can slightly influence the cutoff are considered. Nevertheless, one can see that the data quality is improved compared to the previous results. The maximum of the mirror-correlation coefficients shown in Möbius et al. (2016a) is clearly below 0.900, while with our introduced improvements mirror-correlation coefficients of up to 0.974 are reached. This implies that the curve of the cutoff speed versus ecliptic longitude shows an enhanced symmetry which enables a more precise determination of λ_{flow}. Apparently, the filter for suited IMF directions has a considerable impact on the result for the interstellar flow longitude derived from the PUI cutoff. This is turn means that when accumulating the data over a wide range of IMF configurations, as we did to derive the values displayed in Table 1 and as was performed in Möbius et al. (2016a), the result for λ_{flow} strongly depends on the mix of IMF angles. Additionally, this dependence plays a role in the stochastic error. As every orbit consists of a unique mix of IMF configurations, the cutoff speed in every orbit varies stochastically.

The reason for this dependence must be connected to the torus VDF of freshly injected PUIs and its anisotropy. Furthermore, whatever causes this effect must systematically depend on the combination of ecliptic longitude and IMF as otherwise no asymmetry in the cutoff speeds would be introduced. For example, an effect that would increase the cutoff speed independently of the longitudinal position of STEREO A would just affect the offset parameter in the fit of the model based on Eq. (5) and not λ_{flow}. This argument is, of course, also valid for the fit of the mirror-correlation coefficients. Only if the cutoff is altered together with a longitudinal dependence is the result for λ_{flow} affected.

One possible process that could produce the observed signature is longitudinal transport. As PUIs remain gyrotropic at all times due to the Lorentz-force, their guiding-center velocity depends on the local IMF orientation. If we assume that PUIs are transported towards higher ecliptic longitudes between their time of injection and the time when they are measured, a systematically lower cutoff is determined at $\lambda \approx 150°$ and a systematically higher cutoff is determined at $\lambda \approx 350°$ (Fig. 5c). This would shift the entire cutoff speed curve towards higher ecliptic longitudes and thus an increased value for λ_{flow} would be determined.

One might surmise that under a perfectly perpendicular IMF orientation ($\Phi_{GC} = 0°$) the nominal λ_{flow} would be determined. However, STEREO A's eigen-velocity (which affects the velocity-space coverage of PLASTIC), possible asymmetries of the PUI torus VDF (Drews et al. 2015), and the unknown history of the locally measured IMF transform this into a more involved problem whose individual effects need to be studied separately before being included either in the data selection or through appropriate corrections. Furthermore, PLASTIC's instrument function and, in particular, the efficiency of the position bins that are used to transform the measured speed into the solar wind frame, are complex and not well determined. Hence, we cannot yet exclude that the signature presented in Fig. 6 is caused by the interplay of the complexities of the PUI VDF and PLASTIC's instrument function. For this reason, additional observational constraints and a better understanding of the PUI transport effects will have to be developed. These investigations go beyond the scope of this work and will be included in a separate study in the near future.

8. Conclusion

We have revisited the determination of the interstellar flow longitude based on the PUI cutoff proposed by Möbius et al. (2015). In the first part of this work, we focused on the improvement of the analysis. By using V_r instead of w_{sw} we eliminated a possible systematic influence caused by solar wind speed variations. Another problem that we addressed was the impact of local acceleration sites, which constitute a possible source for systematic uncertainties in the cutoff determination that are stochastically distributed over ecliptic longitude. Thus, they can affect the derivation of λ_{flow} and, of course, increase the uncertainty of the result. By considering the VDF of He^{2+} we were able to exclude them to a large extent.

For the determination of the cutoff speed, we have proposed two new methods, which we show are consistent with the previously used method. A new approach to estimate the error of the analysis was introduced. On the one hand, the statistical error caused by the limited number of He^{+} counts was considered; on the other hand, a stochastic error caused by varying solar wind conditions was taken into account. Both errors were estimated using Monte Carlo approaches. The results of the modified analysis deviate by $\Delta\lambda_{flow} \approx -1°$ from the result presented in Möbius et al. (2016a). This illustrates how the systematic errors that we claim to have minimized, have an impact on the result for λ_{flow}. The resulting stochastic errors of ~0.4° are about one order of magnitude larger than the error presented in Möbius et al. (2015, 2016a) of 0.04°.

Additionally, we found that a direct fit of a model to the data yields an error for the interstellar flow longitude comparable with calculating and fitting mirror-correlation coefficients. The advantage of the direct fit of the cutoff speeds is that the model incorporates the non-circular orbit of STEREO A, which introduces a systematic error in the mirror-correlation approach. Nevertheless, the mirror-correlation coefficients calculated for the cutoff speeds derived from the newly filtered data with the modified methods imply an improved data quality.

Using these improvements, we were able to uncover an unexpected systematic dependence of the derived interstellar flow longitude from the considered IMF configurations. This dependence is not only crucial for determining the actual interstellar flow longitude from the PUI cutoff, but is also very interesting for fundamental PUI transport physics.

This means that the λ_{flow} results of this study displayed in Table 1 and the value presented in Möbius et al. (2016a) are still influenced by the mix of IMF orientations that appear in the selection of the data used to derive these values. At this point, we would like to emphasize that with our current understanding the value of $\lambda_{flow} = 75.41° \pm 0.34°$ with the lowest stochastical uncertainty should not be taken as the real interstellar flow longitude. Our understanding of the involved processes is still not thorough enough to correct for the systematic trend that is introduced by the IMF orientation. Thus, we plan to investigate

possible explanations for this effect in more detail and with a further refinement in the data selection in a follow-up study.

Acknowledgements. This work was supported by the German Space Agency (DLR) under grant number 50 OC 1501, and by the University of Kiel. The work at the University of New Hampshire is supported by SR&T Grant NNX16AF79G. Furthermore, we thank Sonja Taut for her help with Fig. 1a.

References

Acuña, M., Curtis, D., Scheifele, J., et al. 2008, Space Sci. Rev., 136, 203
Axford, W. 1972, NASA SP, 308, 609
Bertaux, J. & Blamont, J. 1971, A&A, 11, 200
Bzowski, M., Kubiak, M., Möbius, E., et al. 2012, ApJS, 198, 12
Chalov, S. 2014, MNRAS, 443, L25
Chotoo, K., Schwadron, N., Mason, G., et al. 2000, J. Geophys. Res., 105, 23107
Drews, C., Berger, L., Wimmer-Schweingruber, R. F., et al. 2010, J. Geophys. Res., 115, A10108
Drews, C., Berger, L., Wimmer-Schweingruber, R. F., et al. 2012, J. Geophys. Res., 117, A09106
Drews, C., Berger, L., Taut, A., Peleikis, T., & Wimmer-Schweingruber, R. 2015, A&A, 575, A97
Drews, C., Berger, L., Taut, A., & Wimmer-Schweingruber, R. F. 2016, A&A, 588, A12
Fahr, H. 1971, Planet. Space Sci., 19, 1121
Fisk, L. & Gloeckler, G. 2012, Space Sci. Rev., 173, 433
Galvin, A., Kistler, L., Popecki, M., et al. 2008, Space Sci. Rev., 136, 437
Gloeckler, G. 1999, in Corotating Interaction Regions (Springer), 91
Gloeckler, G., Geiss, J., Roelof, E., et al. 1994, J. Geophys. Res., 99, 17637
Jian, L., Russell, C., Luhmann, J., & Skoug, R. 2006, Sol. Phys., 239, 337
Kallenbach, R., Geiss, J., Gloeckler, G., & Von Steiger, R. 2000, Ap&SS, 274, 97
McComas, D., Allegrini, F., Bochsler, P., et al. 2009, Science, 326, 959
Möbius, E., Hovestadt, D., Klecker, B., Scholer, M., & Gloeckler, G. 1985, Nature, 318, 426
Möbius, E., Rucinski, D., Hovestadt, D., & Klecker, B. 1995, A&A, 304, 505
Möbius, E., Litvinenko, Y., Grüwaldt, H., et al. 1999, Geophys. Res. Lett., 26, 3181
Möbius, E., Bzowski, M., Chalov, S., et al. 2004, A&A, 426, 897
Möbius, E., Bochsler, P., Bzowski, M., et al. 2012, ApJS, 198, 11
Möbius, E., Lee, M., & Drews, C. 2015, ApJ, 815, 20
Möbius, E., Lee, M., & Drews, C. 2016a, ApJ, 826, 99
Möbius, E., Lee, M., Gloeckler, G., Drews, C., & Keilbach, D. 2016b, in J. Phys. Conf. Ser., 767, 012017
Oka, M., Terasawa, T., Noda, H., Saito, Y., & Mukai, T. 2002, Geophys. Res. Lett., 29, 54
Quinn, P., Schwadron, N., & Möbius, E. 2016, ApJ, 824, 142
Schwadron, N., Fisk, L., & Gloeckler, G. 1996, Geophys. Res. Lett., 23, 2871
Schwadron, N. A., Möbius, E., Leonard, T., et al. 2015, ApJS, 220, 25
Sokół, J. M., Bzowski, M., Kubiak, M. A., & Möbius, E. 2016, MNRAS, 458, 3691
Stone, E., Cummings, A., McDonald, F., et al. 2005, Science, 309, 2017
Taut, A., Berger, L., Bochsler, P., et al. 2016, AIP Conf. Proc., 1720, 050001
Vasyliunas, V. & Siscoe, G. 1976, J. Geophys. Res., 81, 1247
Weller, C. & Meier, R. 1974, ApJ, 193, 471
Witte, M. 2004, A&A, 426, 835
Wood, B. E., Müller, H.-R., & Witte, M. 2015, ApJ, 801, 62